Journal Pre-proof

Dataset on full ultrasonic guided wavefield measurements of a CFRP plate with fully bonded and partially debonded omega stringer

Kudela Pawel, Radzienski Maciej, Moix-Bonet Maria, Willberg Christian, Lugovtsova Yevgeniya, Bulling Jannis, Tschöke Kilian, Moll Jochen

PII: S2352-3409(22)00289-X
DOI: https://doi.org/10.1016/j.dib.2022.108078
Reference: DIB 108078

To appear in: *Data in Brief*

Received date: 5 August 2021
Revised date: 16 March 2022
Accepted date: 17 March 2022

Please cite this article as: Kudela Pawel, Radzienski Maciej, Moix-Bonet Maria, Willberg Christian, Lugovtsova Yevgeniya, Bulling Jannis, Tschöke Kilian, Moll Jochen, Dataset on full ultrasonic guided wavefield measurements of a CFRP plate with fully bonded and partially debonded omega stringer, *Data in Brief* (2022), doi: https://doi.org/10.1016/j.dib.2022.108078

Data in Brief (2022)

Contents lists available at ScienceDirect

Data in Brief

journal homepage: www.elsevier.com/locate/dib

Data Article

Dataset on full ultrasonic guided wavefield measurements of a CFRP plate with fully bonded and partially debonded omega stringer

Kudela Pawel[a,*], Radzienski Maciej[a], Moix-Bonet Maria[b], Willberg Christian[b], Lugovtsova Yevgeniya[c], Bulling Jannis[c], Tschöke Kilian[d], Moll Jochen[e]

[a] *Institute of Fluid Flow Machinery, Polish Academy of Sciences, 80-231 Gdansk, Poland*
[b] *Institute of Composite Structures and Adaptative Systems, German Aerospace Center, 38108 Braunschweig, Germany*
[c] *Federal Institute for Materials Research and Testing (BAM), 12205 Berlin, Germany*
[d] *Fraunhofer Institute for Ceramic Technologies and Systems IKTS, Systems for Condition Monitoring, 01109 Dresden, Germany*
[e] *J.W. Goethe-University, Department of Physics, 60438 Frankfurt, Germany*

ARTICLE INFO

Keywords:

Lamb waves
Composite panel
Impact damage
Damage detection
Scanning laser Doppler vibrometry
Structural Health Monitoring
Non-Destructive Evaluation

ABSTRACT

The fourth dataset dedicated to the Open Guided Waves platform [1] presented in this work aims at a carbon fiber composite plate with an additional omega stringer at constant temperature conditions. The dataset provides full ultrasonic guided wavefields. Two types of signals were used for guided wave excitation, namely chirp signal and tone-burst signal. The chirp signal had a frequency range of 20-500 kHz. The tone-burst signals had a form of sine modulated by Hann window with 5 cycles and carrier frequencies 16.5 kHz, 50 kHz, 100 kHz, 200 kHz and 300 kHz. The piezoceramic actuator used for this purpose was attached to the center of the stringer side surface of the core plate. Three scenarios are provided with this setup: (1) wavefield measurements without damage, (2) wavefield measurements with a local stringer debond and (3) wavefield measurements with a large stringer debond. The defects were caused by impacts performed from the backside of the plate. As result, the stringer feet debonds locally which was verified with conventional ultrasound measurements.

http://dx.doi.org/10.1016/j.dib.xxxx.xx.xxx

Specifications Table

Subject	Mechanical Engineering
Specific subject area	Non-destructive testing, guided wave propagation, full wavefield signal processing
Type of data How data were acquired	Figures, matrices in hdf format Polytec PSV-400 scanning laser Doppler vibrometer;
Data format	Raw
Parameters for data collection	The planar plate dimensions were 0.5 m by 0.5 m whereas the scanning area covered almost the entire surface of the plate excluding the border about 9 mm wide. Measurements were performed in ambient temperature and humidity conditions. Various excitation signals were used, namely, Hann windowed tone-burst signal with 5 cycles and carrier frequencies 16.5 kHz, 50 kHz, 100 kHz, 200 kHz and 300 kHz and chirp signal in the frequency range 20-500 kHz .
Description of data collection	One laser head was used for registration of transverse velocities of guided wave propagation on a surface of a CFRP plate with a stringer while the excitation was performed by using a piezoelectric transducer located at the centre of the plate on the opposite side. The measurements were acquired for the intact plate and after consecutive impacts.
Data source location	Data was obtained at Institute of Fluid-Flow Machinery, Polish Academy of Sciences, Mechanics of Intelligent Structures Department, Gdansk, Poland; Impact was introduced and ultrasonic testing was performed at German Aerospace Center (DLR), Institute of Composite Structures and Adaptive Systems, Braunschweig, Germany
Data accessibility	Data is available at Zenodo platform: Data identification number: 10.5281/zenodo.5105861 Direct URL to data: https://doi.org/10.5281/zenodo.5105861

Value of the Data

- These data provide a data set for elastic guided wave inspection techniques for carbon fibre reinforced polymers with and without an introduced damage. The data thus overcomes the current limitation by a lack of freely available benchmark measurements.
- The development of new guided wave-based techniques and the comparison of existing algorithms require high-quality benchmark measurements. Therefore, all researchers in the field of non-destructive evaluation as well as in the field of guided wave-based monitoring can benefit from these data.
- The data set might be used to evaluate existing signal evaluation techniques, to enable comparisons of evaluation methods and finally to develop new signal evaluation techniques based on elastic guided wave measurements.
- Structural Health Monitoring (SHM) and non-destructive evaluation (NDE) aim to assess the integrity of a structure non-destructively. These research areas are therefore rapidly gaining in importance, and not only due to the increasing digitization of society.
- As importance of ultrasonic guided waves is also growing rapidly, new signal evaluation techniques need to be developed. The provided data set therefore makes an impact in applications ranging from aerospace and automotive to all areas of lightweight construction.

*Corresponding author: pk@imp.gda.pl

1. Data Description

The datasets within this article provide full ultrasonic guided wavefield of a CFRP plate with fully bonded (intact) and partially debonded (impacted) omega stringer measured for various excitation frequencies. The measured datasets [2] are organized as follows:

- *OGW_CFRP_Stringer_Wavefield_Intact*: Baseline wavefield measurements of the intact CFRP plate with the omega stringer
- *OGW_CFRP_Stringer_Wavefield_FirstImpact*: Wavefield measurements of the CFRP plate with the omega stringer impacted with 15.3 J at location [0.38 m, 0.33 m]
- *OGW_CFRP_Stringer_Wavefield_SecondImpact*: Wavefield measurements of the CFRP plate with the omega stringer impacted for the second time with 19 J at location [0.38 m, 0.34 m]

Each folder contains a number of h5-files for two excitation types: Hann-windowed burst and chirp. The folder name for the burst excitation describes the excitation frequency and number of cycles, peak-to-peak voltage used to drive the PZT and number of averages per point used to record the wavefield, *e.g.* **BURST_16_5kHz_5HC_10Vpp_x3** reads as 16.5 kHz centre excitation frequency, 5 cycles Hann-windowed burst, 10 V peak-to-peak and 3 averages per point. The folder name for the chirp excitation describes the excitation frequency range and chirp duration, peak-to-peak voltage used to drive the PZT and number of averages per point used to record the wavefield, *e.g.* **CHIRP_20-500kHz_125us_6Vpp_x3** reads as 20-500 kHz excitation frequency range, 125 µs chirp duration, 6 V peak-to-peak and 3 averages per point. It should be noted that these descriptions correspond to signals coming from a signal generator which were next amplified 20 times by a high voltage amplifier.

To open a h5-file and to see how the h5-files are organized the following options are available:

- HDFView https://support.hdfgroup.org/products/java/hdfview/
- HDF Compass https://github.com/HDFGroup/hdf-compass
- a MATLAB command *h5disp*

In addition, MATLAB and Python scripts are included which can be used to read out the dataset and to visualise the wavefield.

2. Experimental Design, Materials and Methods

2.1. Description of composite panel

The CFRP plate corresponds to the *wave field* plate in [3]. It was manufactured with a dimension of 0.5 m × 0.5 m and a nominal thickness of 2 mm. The corresponding ply thickness is 0.125 mm. The prepreg M21 / 34% / UD134 / T700 / 300 from Hexply ® was used to manufacture the plates with a quasi-isotropic (QI) layup of $[45/0/-45/90/-45/0/45/90]_S$. The material properties of a single unidirectional layer were measured based on standard test procedures [1]. The prepreg M21 / 34% / UD194 / T700 / IMA-12K from Hexply ® was used to separately manufacture the omega stringer. The stringer was built also in a quasi-isotropic layup $[-45/0/90/45/90/-45]_S$ with the dimensions depicted in Figure 1. The nominal thickness

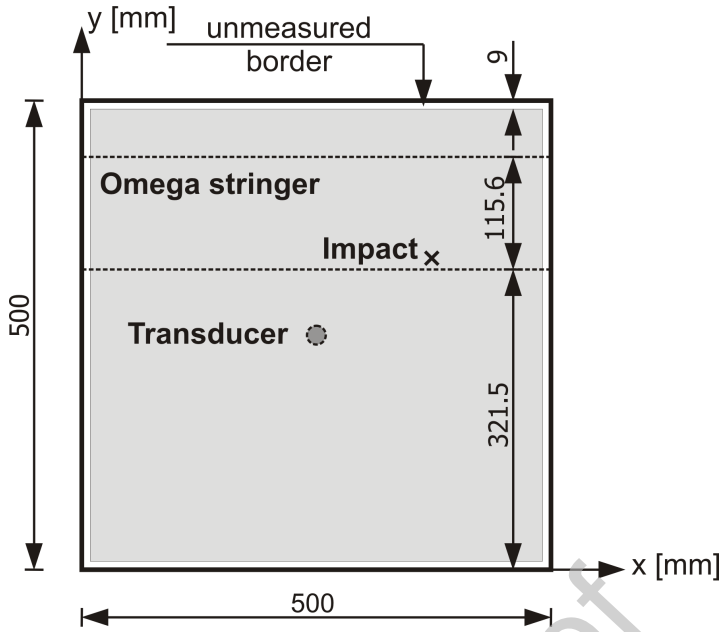

(a) Specimen dimensions and measurement area denoted by grey colour.

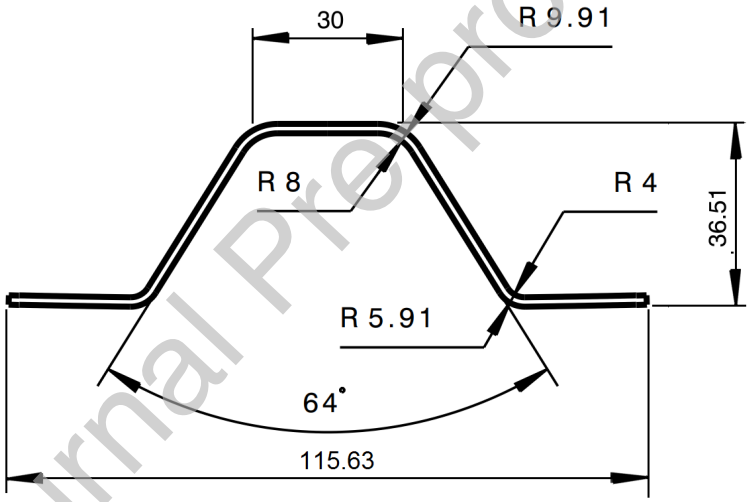

(b) Omega stringer cross-section geometry in mm, taken from [3].

Fig. 1: Plate with omega stringer geometry.

is 1.5 mm with a ply thickness of 0.125 mm. The material properties of plate and stringer are listed in Table 2. The omega stringer was bonded to the plate by using Loctite Hysol 9466. The adhesive was cured in vacuum at room temperature.

Table 2: Stiffness values and density for unidirectional M21 / 34% / UD134 / T700 / 300 material used for the plate, taken from [1], and M21 / 34% / UD194 / IMA-12K as material used for the stringer.

Parameter	M21 / 34% / UD134 / T700 / 300	M21 / 34% / UD194 / IMA-12K
C_{1111} [GPa]	130	174
C_{1122} [GPa]	6.1	4.1
C_{1133} [GPa]	6.1	4.1
C_{2222} [GPa]	11.2	9.6
C_{2233} [GPa]	5.2	2.9
C_{3333} [GPa]	11.2	9.6
C_{1212} [GPa]	3	3.3
C_{2323} [GPa]	4.2	5.9
C_{1313} [GPa]	4.2	5.9
ρ [kg m^{-3}]	1571	1580

A mobile impactor from ID-Lindner has been used to create Barely Visible Impact Damages (BVID) in the specimen. The mobile impactor generates an impact with a defined energy by shooting a metal projectile by means of compressed air. A hemi-spherical projectile with a radius of 25 mm has been employed in order to create BVID. Two impacts have been carried out. The first was executed with an energy of 15.3 J and a speed of 6 m s^{-1} on the coordinates x=0.38 m and y=0.33 m according to Figure 1a. During the second impact the projectile had a speed of 6.7 m s^{-1} and the impact energy of 19 J. The second impact was located 10 mm above the first impact position, with the intention of increasing the damage size.

2.2. Ultrasound NDT measurements

As a reference, non-destructive inspection (NDI) was carried out with the ultrasound equipment USPC 4000 AirTech, from Hillger. Figure 2 displays the C-Scans made after each impact. The colour coding indicates the time-of-flight of the back-wall echo. As observed in Figure 2a, the first impact created a minimal debonding between skin and stringer with dimensions around 12x50mm. After the second impact the debonding grew considerably, affecting both feet of the omega stringer. The large extent of the second impact, with damaged areas far from the impact location, can be explained by the mechanical properties of the specimen. The impact induces a bending load in the specimen. Due to the stiffness of the stringer, the bending load generates large shear forces in the bonded joint. The adhesive layer, probably weakened from the first impact, did not withstand the shear forces during the second impact. The final damage on the specimen is displayed on Figure 2b.

2.3. Data acquisition using scanning laser Doppler vibrometry

Guided waves were excited by a piezoelectric disk of diameter 10 mm attached to the back surface of the specimen (the side with omega stringer). The following excitation signals were applied in consecutive measurements:

- Hann windowed tone-burst signal with 5 cycles and carrier frequencies (f_c) 16.5 kHz, 50 kHz, 100 kHz, 200 kHz, 300 kHz,
- chirp signal in the frequency range 20-500 kHz lasting 200 µs.

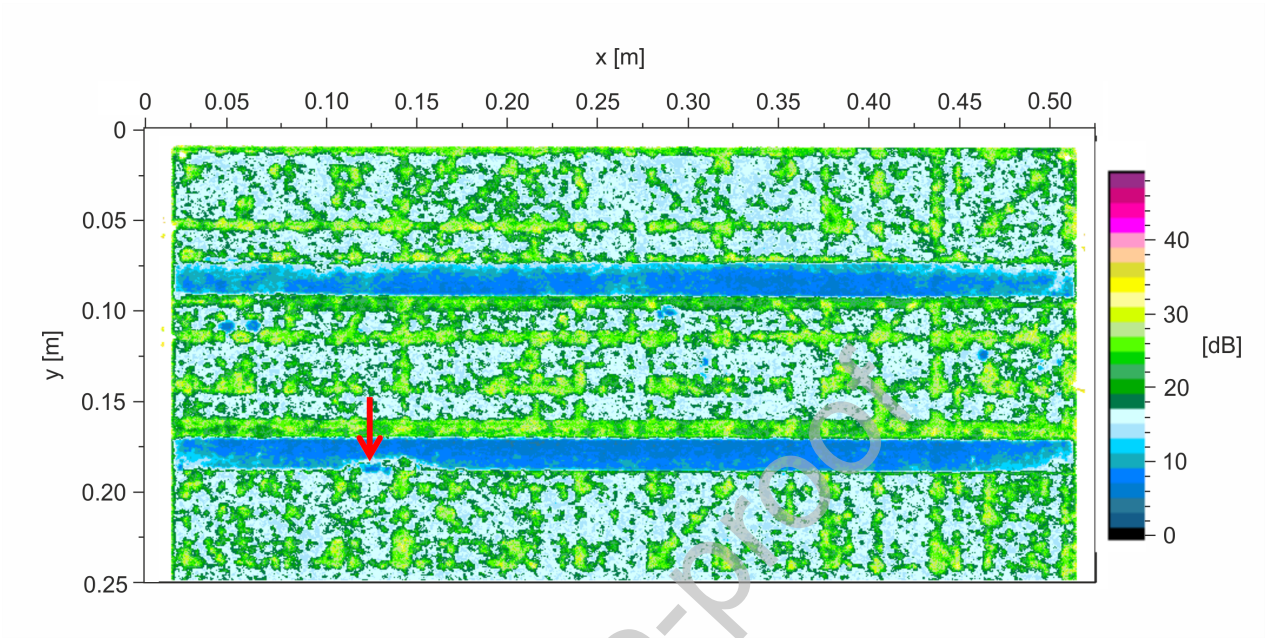

(a) C-Scan after first impact with arrow indicating the impact position

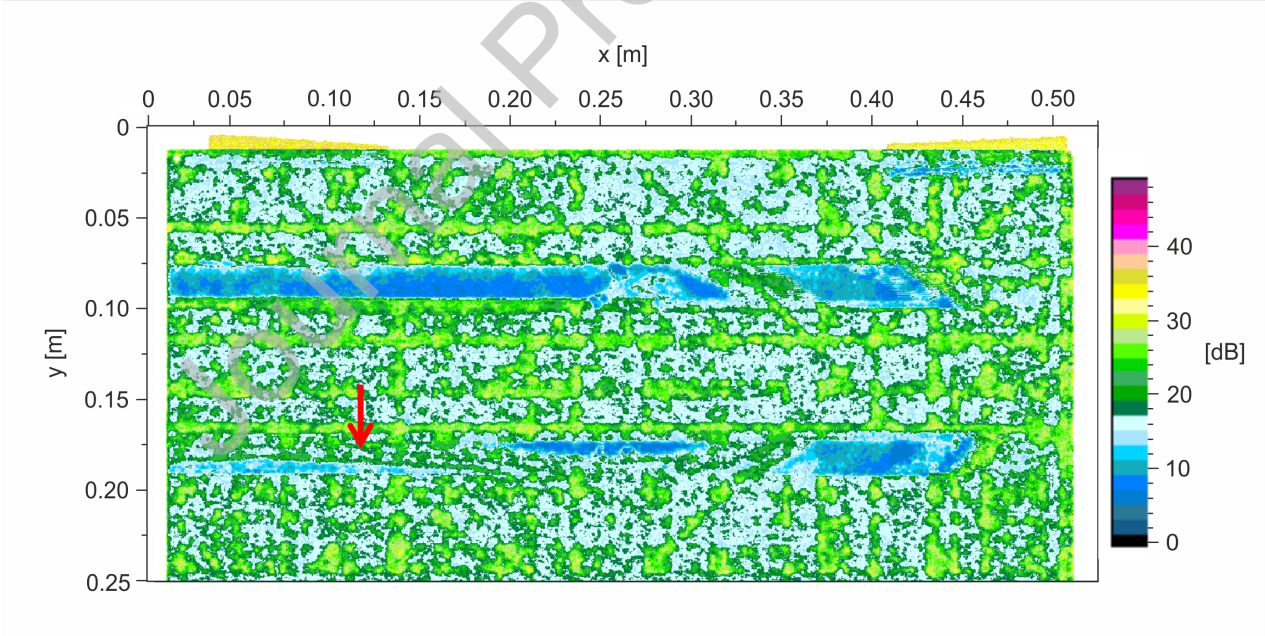

(b) C-Scan after second impact with arrow indicating the impact position

Fig. 2: Ultrasound C-scans after impacts with back-wall echo time-of-flight

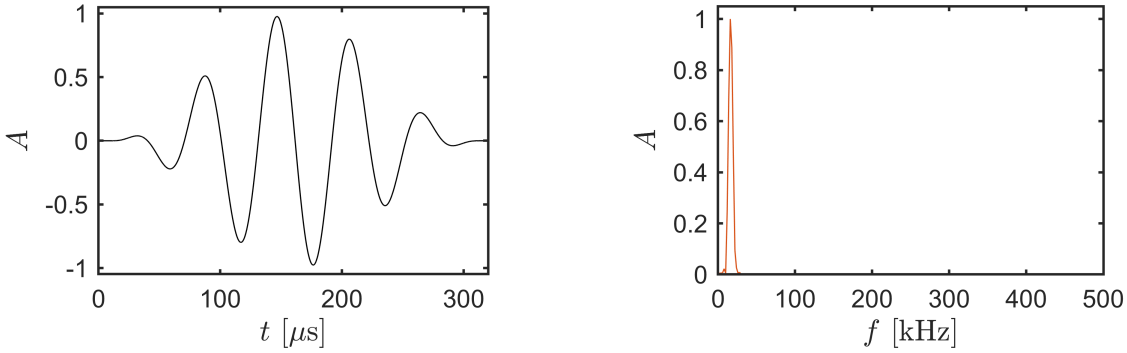

(a) Time domain (b) Frequency domain

Fig. 3: The tone-burst excitation signal for the carrier frequency f_c = 16.5 kHz

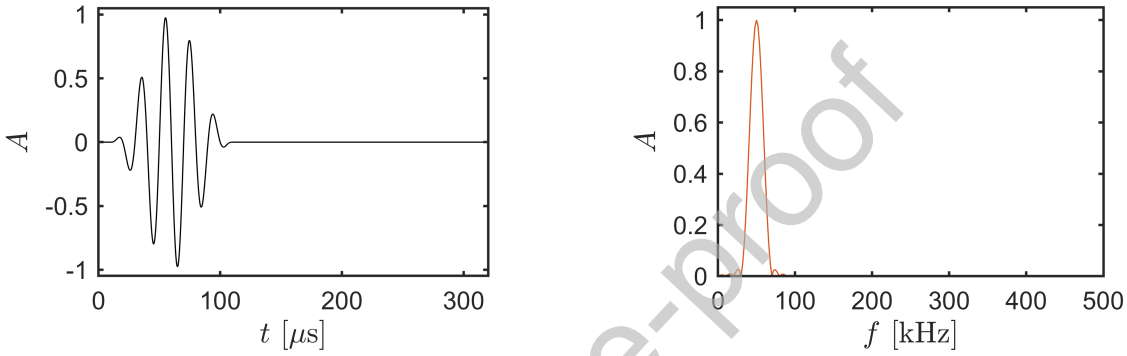

(a) Time domain (b) Frequency domain

Fig. 4: The tone-burst excitation signal for the carrier frequency f_c = 50 kHz

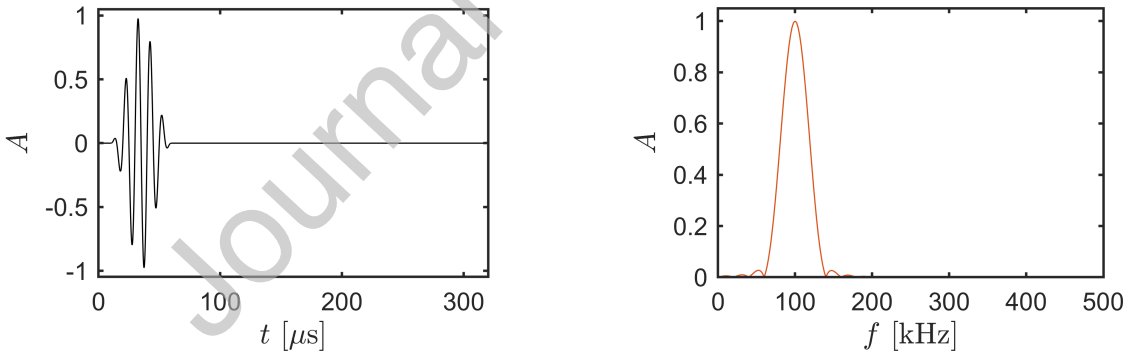

(a) Time domain (b) Frequency domain

Fig. 5: The tone-burst excitation signal for the carrier frequency f_c = 100 kHz

The excitation signals used in this paper are illustrated both in the time and frequency domains in Figures 3-8.

The applied peak to peak voltage at the signal generator varied depending on the type of the signal from 4 V to 11 V. Next, signals were amplified 20 times.

The measurements using scanning laser Doppler vibrometer (SLDV) were conducted on the opposite side of the specimen in respect to the piezoelectric transducer and omega stringer (on the flat surface). The specimen central area excluding border of width about 9 mm was measured

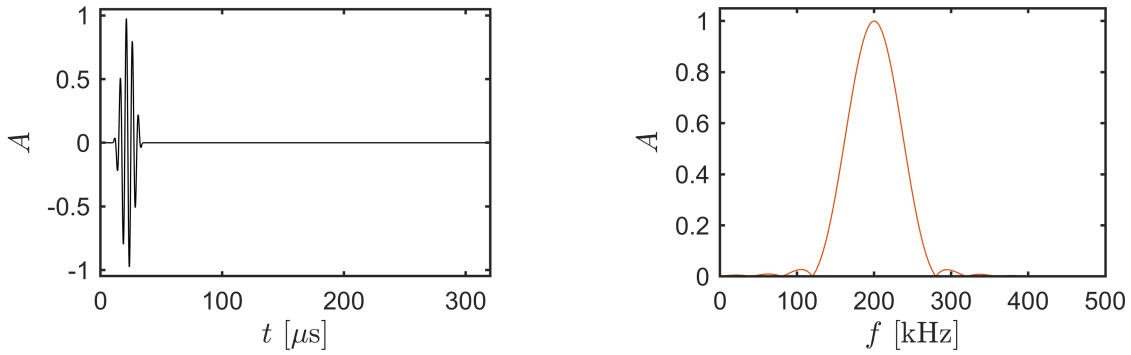

(a) Time domain (b) Frequency domain

Fig. 6: The tone-burst excitation signal for the carrier frequency $f_c = 200$ kHz

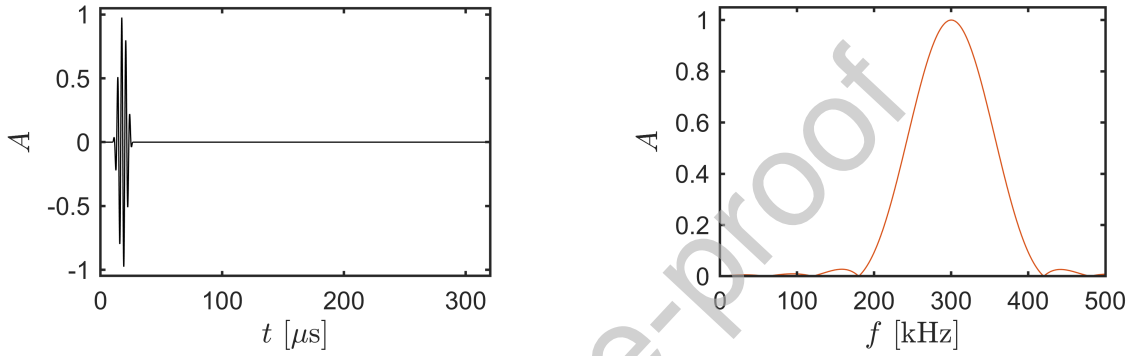

(a) Time domain (b) Frequency domain

Fig. 7: The tone-burst excitation signal for the carrier frequency $f_c = 300$ kHz

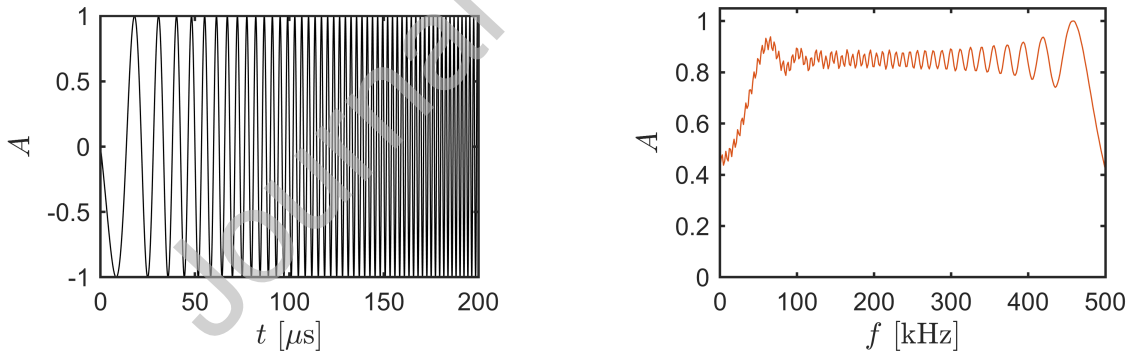

(a) Time domain (b) Frequency domain

Fig. 8: The chirp excitation signal

in 483×483 points. The specimen with highlighted measurement area is presented in Figure 1a. At every measurement point, 1024 time samples were registered for Hann windowed signals and 2048 time samples for chirp signals. The sampling frequency for burst excitation measurements was in range of 256 kHz up to 2.56 MHz chosen from series to be around 10 times higher than f_c. The sampling frequency for chirp excitation was 1.28 MHz.

The measurements were taken 10 times in every grid point and averaged to improve the signal to noise ratio. The exception was the case of Hann windowed tone-burst signal of carrier

frequency 16.5 kHz where only 3 averages were applied. The origin of the coordinate system is located in the lower-left corner of the specimen.

It should be noted that the dataset contains raw signals, however, a band-pass filter embedded in the Polytec data acquisition system was used during measurements. The band-pass cut off frequencies were $f_{cut1} = 0.5 f_c$ and $f_{cut2} = 1.5 f_c$.

2.4. Wavefield animation

Full wavefields of guided waves measured by the scanning laser Doppler vibrometer are of great importance in the field of SHM and NDE. They can be used for validation of various numerical models [4, 5] as well as for development of damage identification algorithms [6, 7, 8, 9, 10]. Hence, our aim is to provide such a dataset so that various methods can be quantitatively compared.

The dataset is accompanied by Matlab script `Read_AcousticWavefield.m` as well as Python scripts `readData.py` and `makeVideo.py` which can be used for reading and visualising data. The scripts should be copied to the desired sub-folder with `*.h5` files so that data will be processed in the current path or alternatively scripts can be modified by including full paths.

Exemplary frames of propagating waves for the case of 100 kHz excitation are presented in Figure 9. Three cases are presented: (i) intact specimen (Figure 9a and Figure 9b), (ii) specimen after first impact (Figure 9c and Figure 9d) and (iii) specimen after second impact. It can be noted that slight differences in the wave pattern caused by the impact appear at 0.15 ms in Figure 9d. In Figure 9e reflection from the stringer is not present which means that the stringer foot debonded from the plate.

2.5. Postprocessing

A simple postprocessing was applied to the acquired full wavefield measurements. The goal is to show that partial debonding of the stringer from the host plate is a challenging problem. Simple signal processing method such as weighted root mean square (WRMS)[6] is not able to highlight the defected area. Only slight changes in the energy distribution are visible as it is presented in Figure 10. Therefore, more advanced signal processing algorithms must be developed and the provided dataset can serve as a benchmark. On the other hand, after second impact, stringer has partially debonded from the plate. Based on WRMS image in Figure 10c it can be concluded that the debonding is extensive - only upper right part of the foot of the stringer remains in contact with the plate.

Another post-processing technique used in this work is a local wavenumber mapping technique introduced by Rogge and Leckey [7] in combination with the one-frequency-approach of Mesnil *et al.* [8]. Wavenumber mapping allows to identify discontinuties in wavenumbers which are caused by local changes in thickness. For instance, a wave travelling in a pristine composite plate will have a different wavenumber than that of a delaminated region. The wavenumber in the damaged region will be equal to that of the plate portion above/below the delamination, when measurement are done on top/bottom.

The necessary steps along with the source code to calculate the wavenumber maps can be found in [9]. The A0-like mode only was used for the analysis due to its sensitivity to the thickness variation. All other modes were filtered out by applying a radial filter in the wavenumber domain leaving the wavenumbers between 350 rad m^{-1} and 750 rad m^{-1} only. The point-wise window size of 31 x 31 bins was applied which corresponds to 31 mm and fulfills the wavenumber resolution criteria of the window size being at least two wavelengths of the expected modes [7]. Moreover, the wavenumber maps were filtered using a median filter of 11 x 11 bins to reduce

the influence of the measurement noise and artefacts. Calculations were done in MATLAB on a 64-bit Windows 10 PC with 32 GB RAM for a wavefield data set which was zero-padded in space to the size of 512 512 x 1024. The computational time for one wavenumber map was about 18 min.

First of all, the transducer is visible in every wavenumber map in the middle of sample having the wavenumber of 520 rad m^{-1}. A typical edge artifact can be observed too. The feet of the stringer are highlighted at positions around $y = 0.33$ m and $y = 0.42$ m with the wavenumber of ≈ 500 rad m^{-1}. Note that the wavenumber for the upper foot are not homogeneous through its length which may indicate the lack of bonding at the discontinuities, *e.g.* see a region at $y = 0.42$ m and $x = 0.18 - 0.24$ m in Figure 11a and 11b. These discontinuities are also partially visible in WRMS maps shown in Figure 10a and 10b. Moreover, the anisotropy of the composite plate becomes apparent in the wavenumber maps, especially for the case of the second impact shown in Figure 11c. The left upper as well as the right bottom quadrants of the map have wavenumbers around 610 rad m^{-1}, whereas the left bottom and right upper quadrants have wavenumbers around 560 rad m^{-1}.

As for the impact damage, the first impact caused only a small delamination in the structure which is hardly recognisable in the wavenumber map, confer Fig. Figure 11a and 11b. A black dot in Figure 11b marks the impact position. The change in the wavenumber between intact structure and the structure after the first impact varies between 5 rad m^{-1} and 29 rad m^{-1}, measured to the right of the impact location at positions $y = 0.33$ m and $x = 0.415$ m, and $y = 0.33$ m and $x = 0.418$ m, respectively. This damage would probably go unnoticed, if one would not know where to look at. The WRMS map shown in Figure 10b gives a better indication of the damage thanks to the scattering of the waves at the delamination. For the case of the second impact, both WRMS (Figure 10c) and wavenumber (Figure 11c) maps indicated the debonding of the whole bottom foot and the left half of the upper foot. All in all, for the case presented here, the only difference of wavenumber mapping over WRMS is additional information provided about the plate's anisotropy.

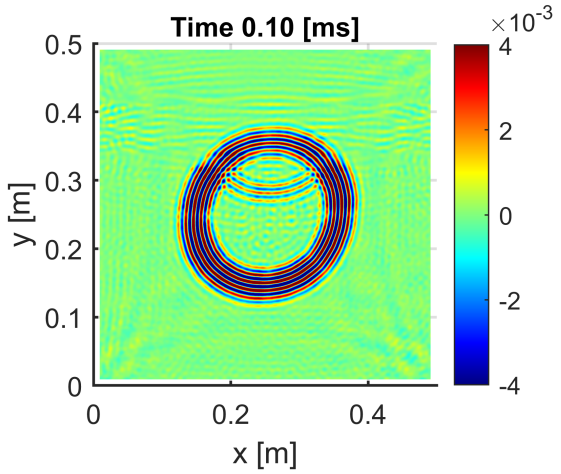

(a) Intact, 0.10 ms

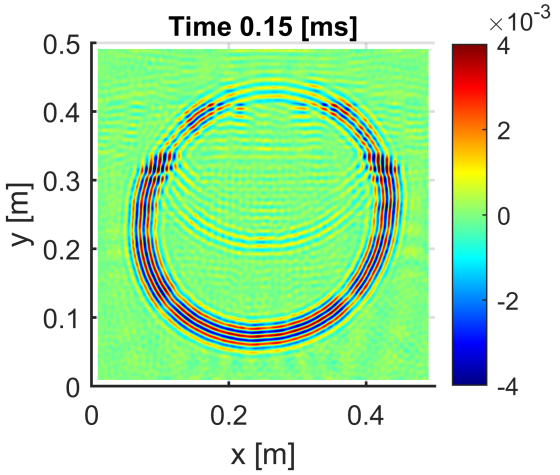

(b) Intact, 0.15 ms

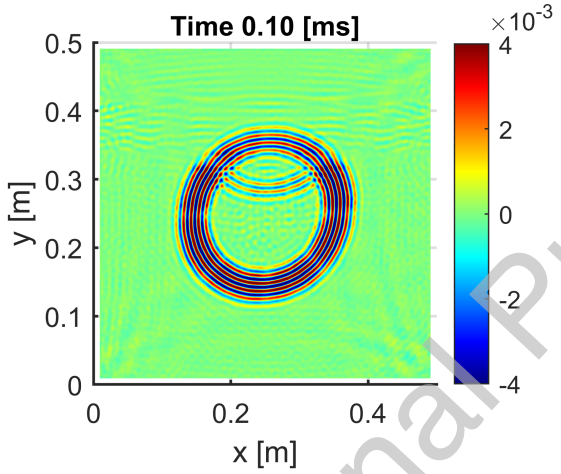

(c) First impact, 0.10 ms

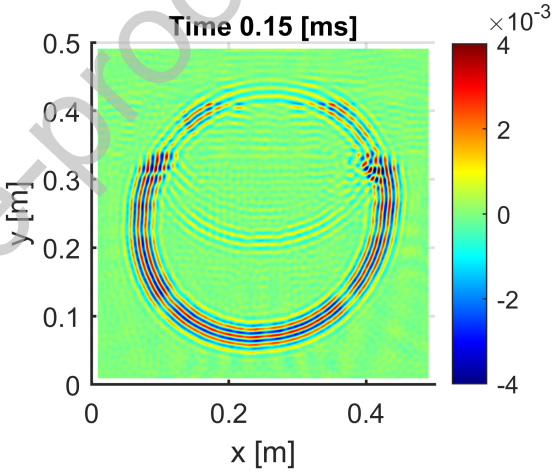

(d) First impact, 0.15 ms

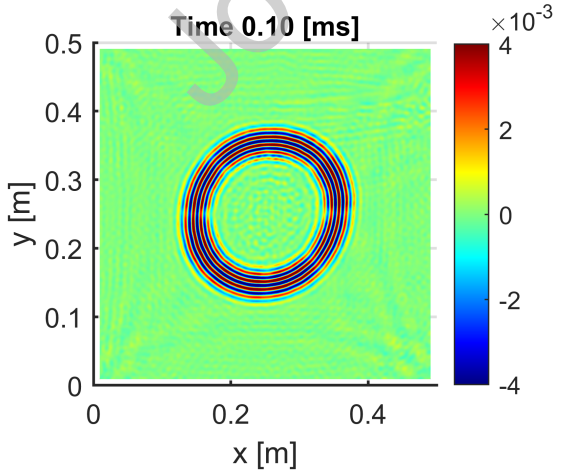

(e) Second impact, 0.10 ms

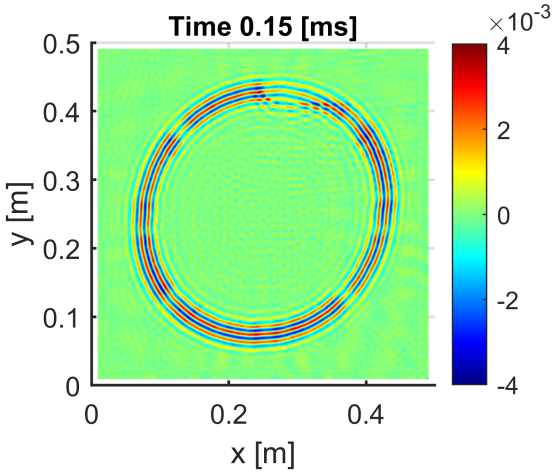

(f) Second impact, 0.15 ms

Fig. 9: Exemplary frames of propagating waves for the case of intact plate, first impact and second impact.

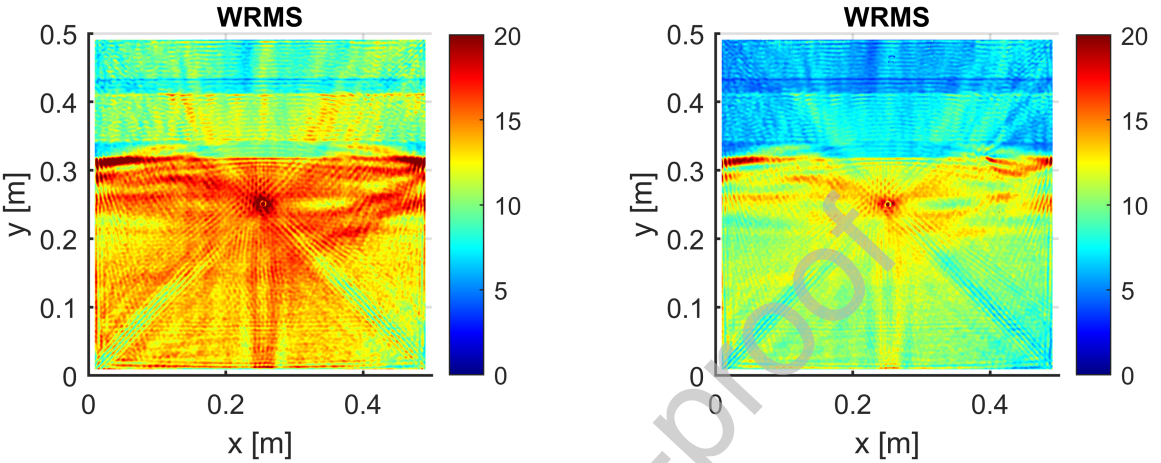

(a) WRMS intact

(b) WRMS first impact

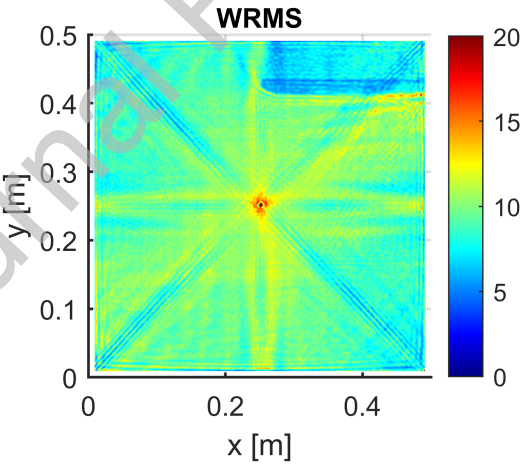

(c) WRMS second impact

Fig. 10: WRMS showing energy distribution for the case of intact plate, first impact and second impact.

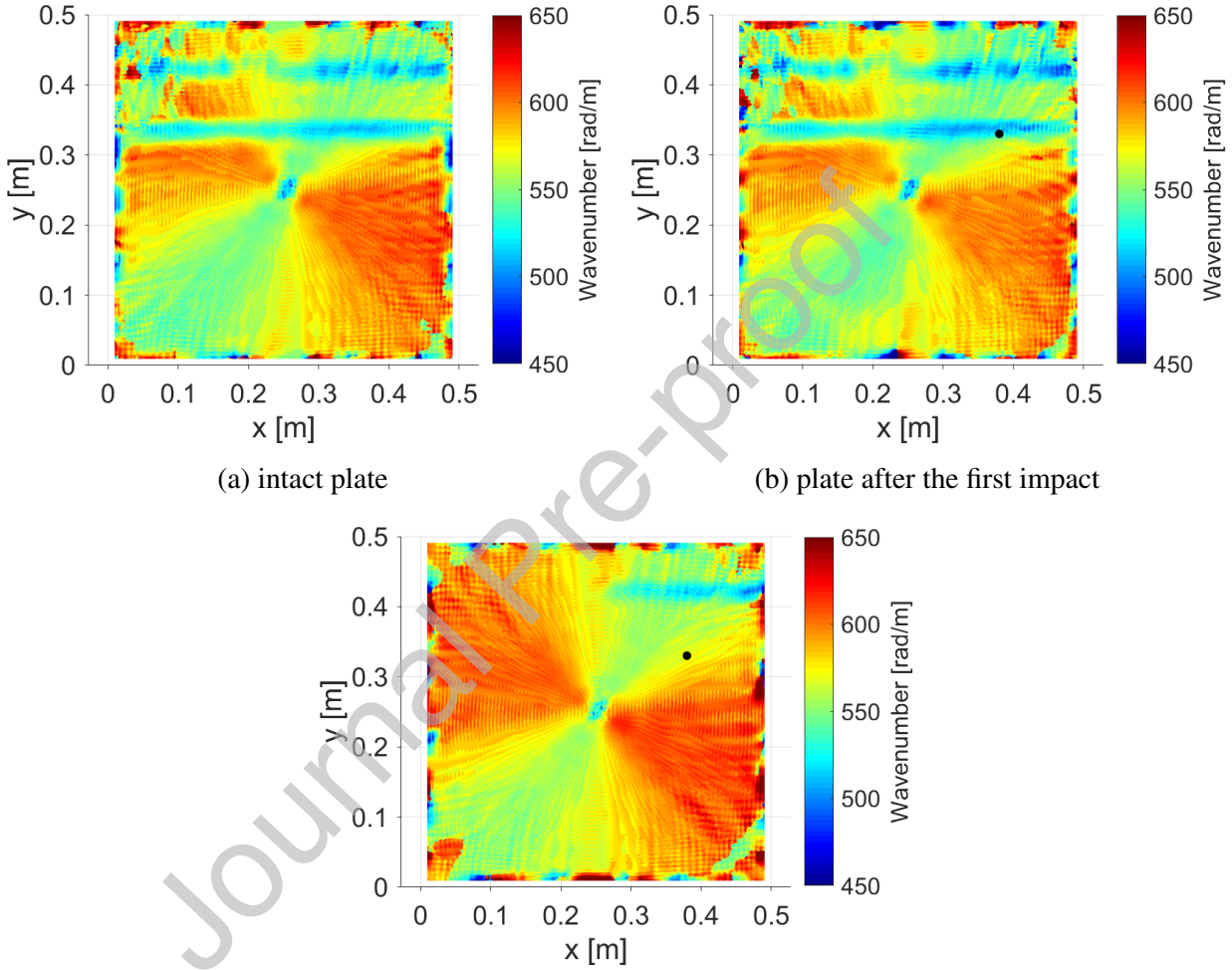

(a) intact plate

(b) plate after the first impact

(c) plate after the second impact

Fig. 11: Local wavenumber maps at 100 kHz calculated from the wavefield measurements at the same excitation frequency. A black dot marks the position of the impact.

Acknowledgments

Pawel Kudela would like to thank the Polish National Science Center for the finance support under grant agreement no. 2018/31/B/ST8/00454. Jannis Bulling gratefully acknowledges the German Research Foundation for funding (DFG project number 428590437).

Declaration of Competing Interest

The authors declare that they have no known competing financial interests or personal relationships which have, or could be perceived to have, influenced the work reported in this article.

CRediT authorship contribution statement

Pawel Kudela: Funding acquisition, Supervision, Project administration, Software, Visualization, Data Curation, Writing - Original Draft, Writing - Review & Editing. **Maciej Radzienski**: Investigation, Validation, Writing - Original Draft, Writing - Review & Editing. **Maria Moix-Bonet**: Investigation, Visualization, Data Curation, Writing - Original Draft, Writing - Review & Editing. **Christian Wilberg**: Software, Validation, Writing - Original Draft, Writing - Review & Editing. **Yevgeniya Lugovtsova**: Investigation, Visualization, Writing - Original Draft, Writing - Review & Editing. **Jannis Bulling**: Funding acquisition, Investigation, Data Curation, Writing - Original Draft, Writing - Review & Editing. **Kilian Tschöke**: Investigation, Data Curation, Writing - Original Draft, Writing - Review & Editing. **Jochen Moll**: Conceptualization, Supervision, Methodology, Writing - Original Draft, Writing - Review & Editing.

References

[1] J. Moll, J. Kathol, C.-P. Fritzen, M. Moix-Bonet, M. Rennoch, M. Koerdt, A. S. Herrmann, M. G. R. Sause, M. Bach, Open Guided Waves - Online Platform for Ultrasonic Guided Wave Measurements, Structural Health Monitoring 18 (2019) 1903–1914.

[2] P. Kudela, M. Radzienski, M. Moix-Bonet, C. Willberg, Y. Lugovtsova, J. Bulling, K. Tschöke, J. Moll, Dataset on full ultrasonic guided wavefield measurements of a CFRP plate with fully bonded and partially debonded omega stringer (1.0) [data set], Zenodo (2021).

[3] J. Moll, C. Kexel, J. Kathol, C.-P. Fritzen, M. Moix-Bonet, C. Willberg, M. Rennoch, M. Koerdt, A. Herrmann, Guided waves for damage detection in complex composite structures: The influence of omega stringer and different reference damage size, Applied Sciences 10 (2020).

[4] Y. Shen, C. E. Cesnik, Hybrid local FEM/global LISA modeling of damped guided wave propagation in complex composite structures, Smart Materials and Structures 25 (2016).

[5] P. Kudela, J. Moll, P. Fiborek, Parallel spectral element method for guided wave based structural health monitoring, Smart Materials and Structures 29 (2020) 095010.

[6] M. Radzieński, Ł. Doliński, M. Krawczuk, A. Żak, W. Ostachowicz, Application of RMS for damage detection by guided elastic waves, Journal of Physics: Conference Series 305 (2011) 012085.

[7] M. D. Rogge, C. A. Leckey, Characterization of impact damage in composite laminates using guided wavefield imaging and local wavenumber domain analysis, Ultrasonics 53 (2013) 1217–1226.

[8] O. Mesnil, C. A. Leckey, M. Ruzzene, Instantaneous and local wavenumber estimations for damage quantification in composites, Structural Health Monitoring 14 (2015) 193–204.

[9] Y. Lugovtsova, J. Bulling, O. Mesnil, J. Prager, D. Gohlke, C. Boller, Damage quantification in an aluminium-cfrp composite structure using guided wave wavenumber mapping: Comparison of instantaneous and local wavenumber analyses, NDT & E International 122 (2021) 102472.

[10] W. J. Staszewski, R. B. Jenal, A. Klepka, M. Szwedo, T. Uhl, A review of laser doppler vibrometry for structural health monitoring applications, Key Engineering Materials 518 (2012) 1–15.